25th ABCM International Congress of Mechanical Engineering
October 20-25, 2019, Uberlândia, MG, Brazil

DESIGN AND CONTROL OF A 2-DOF PARALLEL MECHANISM

André Garnier Coutinho
Victor Pacheco Bartholomeu
Isabella Stevani
Juliana Martins de Oliveira-Fuess
Tarcisio Antonio Hess-Coelho
Diego Colón
Escola Politécnica, Universidade de São Paulo – Cidade Universitária, São Paulo, Brazil
andre.garnier.coutinho@usp.br, victor.bartholomeu@usp.br, isabella.stevani@usp.br, juliana.oliveira465@gmail.com, tarchess@usp.br, diego@lac.usp.br

Abstract. *The study of robotic mechanisms with parallel architecture has been increasing in recent years due to their lower inertia, higher accuracy, precision and greater rigidity in comparison to serial ones. However, the inherent complexity in obtaining a dynamic model restricts the feasibility of implementing model-based control methods such as the computed-torque control (CTC). In this paper, a systematic method for dynamic modeling of closed-chain robots is applied to a 2-DOF parallel mechanism. Essentially, the method couples the dynamic model of each serial subsystem that composes the parallel mechanism through mechanical constraints obtained from the robot kinematics. In addition, a construction approach focused on reducing movement direction clearances is performed by placing all joints in the direction the mechanism is not expected to move. For testing and validation, simulation and experimental results are obtained and compared by applying a model-based control law, such as CTC, and a non-model-based law, such as a simple PD with feed-forward. As expected, the model-based control showed lower regime errors than the PD at the cost of a small increase in energy expenditure.*

Keywords: *parallel mechanism, robotics, dynamic modeling, robot construction, nonlinear control*

1. INTRODUCTION

Parallel mechanisms have been increasingly used in tasks such as pick-and-place operations, machining, flight simulators, positioning telescopes, among others. The main features that can be attractive for the accomplishment of these tasks are the high load capacity, positioning accuracy, structural rigidity and low inertia, which allows high speeds and accelerations to be achieved (Cheng *et al.*, 2003; Khalil and Dombre, 2004; Merlet, 2002; Pashkevich *et al.*, 2006; Tsai, 1999). However, these promising features come at the cost of a smaller workspace and a much more coupled and nonlinear dynamics when compared to equivalent serial mechanisms (Almeida, 2013; Merlet, 2002).

Several formulations for the dynamic modeling of parallel mechanisms are found in the literature. The formalism of Newton-Euler (Arian *et al.*, 2017; Dasgupta and Mruthyunjaya, 1998; Li *et al.*, 2003; Shiau *et al.*, 2008; Zhang *et al.*, 2014) and Lagrange (Li and Xu, 2005; Singh and Santhakumar, 2015; Singh *et al.*, 2015, 2014; Yao *et al.*, 2017) can be pointed out as ones of the most used. However, there are inherent difficulties in such methods that make them inefficient: for example, the need for calculations of reactive efforts and the usage of multipliers, respectively. Other popular choices for the dynamic modeling of parallel robots are the Virtual Work Principle (VWP) and the Virtual Power Principle (Codourey, 1996; Codourey and Burdet, 1997; Gallardo-Alvarado *et al.*, 2018; Geike and McPhee, 2003; Li and Staicu, 2012; Li and Xu, 2009; Staicu, 2009a,c,b; Carp-Ciocardia *et al.*, 2003; Staicu *et al.*, 2007; Staicu and Zhang, 2008; Staicu *et al.*, 2006; Wu *et al.*, 2009; Zhao and Gao, 2009b,a; Zhu *et al.*, 2005). Although they avoid the calculation of reactive efforts, many of these methodologies rely on complex mathematical manipulations or simplifying hypotheses. Also, it is worth mentioning the works that use the Boltzmann-Hamel formalism (Abdellatif and Heimann, 2009; Altuzarra *et al.*, 2015) and the natural orthogonal complement formulation (NOC) (Akbarzadeh *et al.*, 2013; Khan *et al.*, 2005; Xi and Sinatra, 2002), which can be very promising, either by enabling reuse of preconceived models or by avoiding the calculation of reactive efforts.

In this work, a generic formulation inspired by the work of Orsino (Orsino, 2016; Orsino and Hess-Coelho, 2015; Orsino *et al.*, 2015) is proposed based on the Virtual Work Principle and the subsystem coupling principle, allowing the reuse of preconceived models. The formulation is used to compute the dynamic modeling of a 2-DOF parallel mechanism of articulated pentagon type. Direct dynamic simulation of this mechanism is performed using the CTC law (Craig, 2005). In order to show that the obtained model is indeed suitable for the implementation of model based control techniques, experimental essays are performed comparing the performance of the model based CTC law, using the deduced model, and the non-model based Proportional Derivative control law (PD).

2. MODELING

The systematic methodology proposed here to compute closed-chain mechanisms' kinematic and dynamic models was developed based on Orsino *et al.* (2015); Orsino (2016); Orsino and Hess-Coelho (2015). It can be divided into two main steps: the fragmentation of the parallel system into serial subsystems and the assembly of these subsystems through mechanical constraints obtained from the parallel robot kinematics. In the specific case of the pentagon parallel mechanism (Figure 1a), the system is fragmented into two RR serial mechanisms combined through four constraint equations, leading to a 2-DOF mechanism.

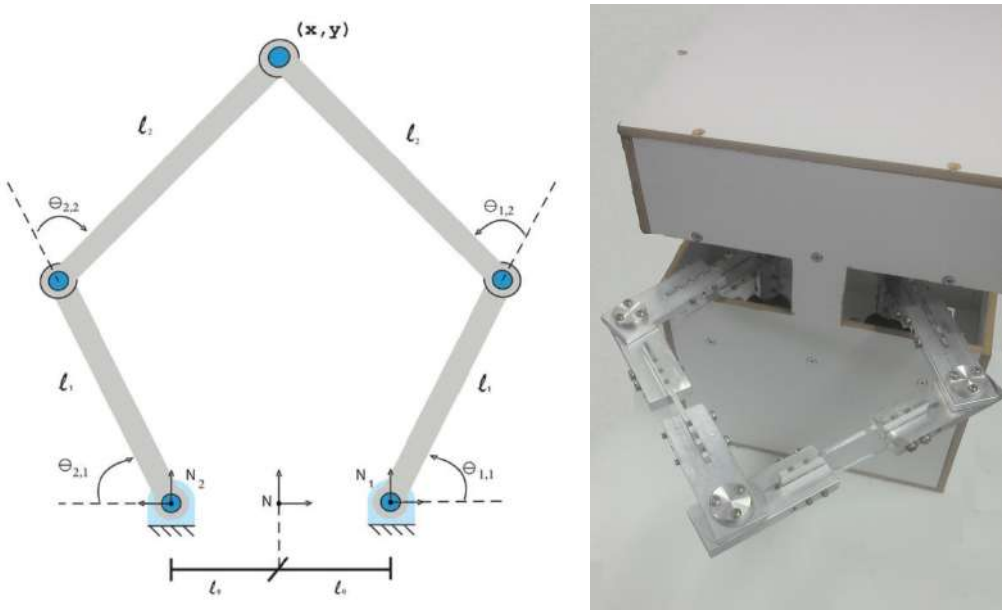

(a) Schematics. **(b)** Construction.

Figure 1: 2-DOF parallel mechanism.

2.1 Forward Kinematics

In order to obtain the end-effector's coordinates in terms of the joint angles, there are two possible paths in the parallel architecture described in Figure 1a: one beginning at the right link and the other at the left one. Since the end-effector's coordinates must satisfy both paths, they could be combined into:

$$\bar{\boldsymbol{q}}(\boldsymbol{q}) = \begin{bmatrix} x - (l_0 + l_1\mathsf{c}\theta_{1,1} + l_2\mathsf{c}\theta_{1,1+2}) \\ y - (l_1\mathsf{s}\theta_{1,1} + l_2\mathsf{s}\theta_{1,1+2}) \\ x - (-l_0 - l_1\mathsf{c}\theta_{2,1} - l_2\mathsf{c}\theta_{2,1+2}) \\ y - (l_1\mathsf{s}\theta_{2,1} + l_2\mathsf{s}\theta_{2,1+2}) \end{bmatrix} = \mathbf{0} \text{ with } \boldsymbol{q} = \begin{bmatrix} x \\ y \\ \theta_{1,1} \\ \theta_{1,2} \\ \theta_{2,1} \\ \theta_{2,2} \end{bmatrix}, \tag{1}$$

where $\boldsymbol{q}$ stands for the generalized coordinates vector, l_j [m] is the j^{th} link length, (x, y) [m] are the end-effector's coordinates and $\theta_{i,j}$ [rad] is the j^{th} link joint angle with respect to the i^{th} kinematic chain. Also, $\mathsf{s}(x)$ and $\mathsf{c}(x)$ states for $\sin(x)$ and $\cos(x)$, respectively, and $\theta_{a,b+c}$ states for $\theta_{a,b} + \theta_{a,c}$.

Through Eq. (1), its first variation can be computed, resulting in the system's direct kinematics:

$$\delta\bar{\boldsymbol{q}}(\boldsymbol{q}) = \boldsymbol{A}(\boldsymbol{q})\delta\boldsymbol{q} = \mathbf{0} \tag{2}$$

$$\text{with } \boldsymbol{A}(\boldsymbol{q}) = \frac{\partial\bar{\boldsymbol{q}}}{\partial\boldsymbol{q}} = \begin{bmatrix} 1 & 0 & l_1\mathsf{s}\theta_{1,1} + l_2\mathsf{s}\theta_{1,1+2} & l_2\mathsf{s}\theta_{1,1+2} & 0 & 0 \\ 0 & 1 & -l_1\mathsf{c}\theta_{1,1} - l_2\mathsf{c}_{1,1+2} & 0 & 0 & 0 \\ 1 & 0 & 0 & 0 & -l_1\mathsf{s}\theta_{2,1} - l_2\mathsf{s}\theta_{2,1+2} & -l_2\mathsf{s}\theta_{2,1+2} \\ 0 & 1 & 0 & 0 & -l_1\mathsf{c}\theta_{2,1} - l_2\mathsf{c}\theta_{2,1+2} & -l_2\mathsf{c}\theta_{2,1+2} \end{bmatrix} \tag{3}$$

The generalized coordinates vector $\boldsymbol{q}$ could be split into actuated and passive coordinates:

$$\boldsymbol{q} = \boldsymbol{Q_a q_a} + \boldsymbol{Q_p q_p} \text{ with } \boldsymbol{Q_a} = \begin{bmatrix} 0 & 0 \\ 0 & 0 \\ 1 & 0 \\ 0 & 0 \\ 0 & 1 \\ 0 & 0 \end{bmatrix}, \boldsymbol{Q_p} = \begin{bmatrix} 1 & 0 & 0 & 0 \\ 0 & 1 & 0 & 0 \\ 0 & 0 & 0 & 0 \\ 0 & 0 & 1 & 0 \\ 0 & 0 & 0 & 0 \\ 0 & 0 & 0 & 1 \end{bmatrix}, \boldsymbol{q_a} = \begin{bmatrix} \theta_{1,1} \\ \theta_{2,1} \end{bmatrix}, \boldsymbol{q_p} = \begin{bmatrix} x \\ y \\ \theta_{1,2} \\ \theta_{2,2} \end{bmatrix}. \tag{4}$$

Splitting its first variation as well and substituting it in (2) results, after some manipulation, in:

$$\delta\boldsymbol{q} = \boldsymbol{C}(\boldsymbol{q})\delta\boldsymbol{q_a} \text{ with } \boldsymbol{C} = \boldsymbol{Q_a} - \boldsymbol{Q_p}(\boldsymbol{AQ_p})^{-1}\boldsymbol{AQ_a}, \tag{5}$$

which will be used together with $\boldsymbol{A}(\boldsymbol{q})$ to compute the system dynamics.

2.2 Singular loci

In order to obtain the singular loci of the mechanism's workspace, the generalized coordinates vector $\boldsymbol{q}$ is also splited into 2 other vector, the task coordinates $\boldsymbol{q_x}$ and the non-task coordinates $\boldsymbol{q_{\bar{x}}}$:

$$\boldsymbol{q} = \boldsymbol{Q_x q_x} + \boldsymbol{Q_{\bar{x}} q_{\bar{x}}} \text{ with } \boldsymbol{Q_x} = \begin{bmatrix} 1 & 0 \\ 0 & 1 \\ 0 & 0 \\ 0 & 0 \\ 0 & 0 \\ 0 & 0 \end{bmatrix}, \boldsymbol{Q_{\bar{x}}} = \begin{bmatrix} 0 & 0 & 0 & 0 \\ 0 & 0 & 0 & 0 \\ 1 & 0 & 0 & 0 \\ 0 & 1 & 0 & 0 \\ 0 & 0 & 1 & 0 \\ 0 & 0 & 0 & 1 \end{bmatrix}, \boldsymbol{q_x} = \begin{bmatrix} x \\ y \end{bmatrix}, \boldsymbol{q_{\bar{x}}} = \begin{bmatrix} \theta_{1,1} \\ \theta_{1,2} \\ \theta_{2,1} \\ \theta_{2,2} \end{bmatrix}. \tag{6}$$

Substituing (4) in (2) and also (6) in (2), the variations $\delta\boldsymbol{q_p}$ and $\delta\boldsymbol{q_{\bar{x}}}$ can be obteined in funcion of $\delta\boldsymbol{q_a}$ and $\delta\boldsymbol{q_x}$, respectively:

$$\delta\boldsymbol{q_p} = -(\boldsymbol{AQ_p})^{-1}\boldsymbol{Q_a A}\delta\boldsymbol{q_a} \tag{7}$$

$$\delta\boldsymbol{q_{\bar{x}}} = -(\boldsymbol{AQ_{\bar{x}}})^{-1}\boldsymbol{Q_x A}\delta\boldsymbol{q_x} \tag{8}$$

The singularities occur when the matrix $\boldsymbol{AQ_p}$ or the matrix $\boldsymbol{AQ_{\bar{x}}}$ is singular. In figure 2, the singular loci was obtained numerically, being the points of the workspace with $|\det \boldsymbol{AQ_p}| \leq \epsilon_a$ or $|\det \boldsymbol{AQ_{\bar{x}}}| \leq \epsilon_x$, whith $\epsilon_a = 10^{-11}$ and $\epsilon_x = 1.6 \cdot 10^{-6}$.

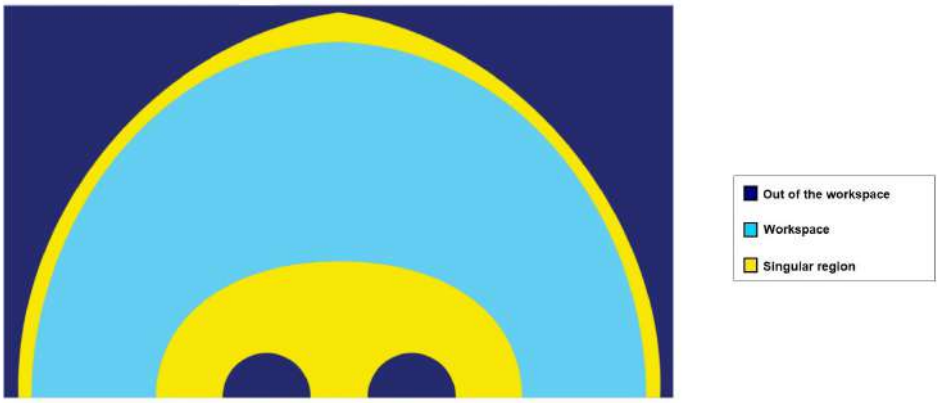

Figure 2: Mechanism workspace.

2.3 Forward Dynamics

According to Orsino *et al.* (2016), it is possible to obtain the dynamic model of a mechanical system from the models of its subsystems and the links between them.

As can be seen in Tarcisio A.H. Coelho (2004), the dynamic model of the i^{th} RR serial mechanism is given by:

$$\boldsymbol{M_i}(\boldsymbol{q_i})\ddot{\boldsymbol{q}}_{\boldsymbol{i}} + \boldsymbol{v_i}(\boldsymbol{q_i}, \dot{\boldsymbol{q}}_{\boldsymbol{i}}) + \boldsymbol{g_i}(\boldsymbol{q_i}) = \boldsymbol{u_i} \text{ with} \tag{9}$$

$$\boldsymbol{M_i} = \begin{bmatrix} D_{11}^{(i)} & D_{12}^{(i)} \\ D_{12}^{(i)} & D_{22}^{(i)} \end{bmatrix}, \boldsymbol{v_i} = \begin{bmatrix} D_{111}^{(i)}\dot{\theta}_{i,1}^2 + D_{122}^{(i)}\dot{\theta}_{i,2}^2 + D_{112}^{(i)}\dot{\theta}_{i,1}\dot{\theta}_{i,2} + D_{121}^{(i)}\dot{\theta}_{i,1}\dot{\theta}_{i,2} \\ D_{211}^{(i)}\dot{\theta}_{i,1}^2 + D_{222}^{(i)}\dot{\theta}_{i,2}^2 + D_{212}^{(i)}\dot{\theta}_{i,1}\dot{\theta}_{i,2} + D_{221}^{(i)}\dot{\theta}_{i,1}\dot{\theta}_{i,2} \end{bmatrix}, \boldsymbol{g_i} = \begin{bmatrix} D_1^{(i)} \\ D_2^{(i)} \end{bmatrix}, \boldsymbol{q_i} = \begin{bmatrix} \theta_{i,1} \\ \theta_{i,2} \end{bmatrix}, \boldsymbol{u_i} = \begin{bmatrix} u_{i,1} \\ u_{i,2} \end{bmatrix} \tag{10}$$

$$D_{11}^{(i)} = m_1^{(i)} l_{g1}^{2\,(i)} + I_1^{(i)} + m_2^{(i)}(l_1^{2\,(i)} + l_{g2}^{2\,(i)}) + I_2^{(i)} + 2m_2^{(i)} l_1^{(i)} l_{g2}^{(i)} \mathsf{c}\theta_{i,2} \tag{11}$$

$$D_{21}^{(i)} = D_{12}^{(i)} = m_2^{(i)} l_{g2}^{2\,(i)} + I_2^{(i)} + m_2^{(i)} l_1^{(i)} l_{g2}^{(i)} \mathsf{c}\theta_{i,2} \tag{12}$$

$$D_{111}^{(i)} = D_{222}^{(i)} = D_{212}^{(i)} = D_{221}^{(i)} = 0 \tag{13}$$

$$D_{112}^{(i)} = D_{121}^{(i)} = D_{122}^{(i)} = -m_2^{(i)} l_1^{(i)} l_{g2}^{(i)} \mathsf{s}\theta_{i,2} \tag{14}$$

$$D_{22}^{(i)} = m_2^{(i)} l_{g2}^{2\,(i)} + I_2^{(i)} \tag{15}$$

$$D_{211}^{(i)} = m_2^{(i)} l_1^{(i)} l_{g2}^{(i)} \mathsf{s}\theta_{i,2} \tag{16}$$

$$D_1^{(i)} = (m_1^{(i)} l_{g1}^{(i)} + m_2^{(i)} l_1^{(i)}) g\, \mathsf{c}\theta_{i,1} + m_2^{(i)} l_{g2}^{(i)} g\, \mathsf{c}\theta_{i,1+2} \tag{17}$$

$$D_2^{(i)} = m_2^{(i)} l_{g2}^{(i)} g\, \mathsf{c}\theta_{i,1+2} \tag{18}$$

where $\boldsymbol{M_i}(\boldsymbol{q_i})$ is the inertia matrix, $\boldsymbol{v_i}(\boldsymbol{q_i}, \dot{\boldsymbol{q}}_{\boldsymbol{i}})$ is the vector of centrifugal and Coriolis terms, $\boldsymbol{g_i}(\boldsymbol{q_i})$ is the vector of gravitational forces and $\boldsymbol{u_i}$ is the vector of generalized actuators' efforts (see (Craig, 2005)). Also, lg_j [m] is the distance from the beginning of the j^{th} link to its center of mass, m_j [kg] is the j^{th} link mass, the principal moments of inertia I_j [kg.m^2] of the j^{th} link in relation of its center of mass and g it the gravitational constant [1]. The coefficients of $\boldsymbol{M_i}(\boldsymbol{q_i})$, $\boldsymbol{v_i}(\boldsymbol{q_i}, \dot{\boldsymbol{q}}_{\boldsymbol{i}})$ and $\boldsymbol{g_i}(\boldsymbol{q_i})$ can be easily obtained through the Lagrangian formalism. More details can be found in Lanczos (2012).

Each vector $\boldsymbol{u_i}$ can be decomposed into two parts, the active forces generated by the actuators ($\boldsymbol{\tau_i}$), and the frictional forces generated by the actuators bearings. Considering that friction has a viscous friction portion and another Coulomb friction portion, the decomposition becomes:

$$\boldsymbol{u_i} = \boldsymbol{\tau_i} - \underline{b}_i\, \dot{\boldsymbol{q}}_{\boldsymbol{i}} - \underline{\mu}_i\, \mathsf{sign}(\dot{\boldsymbol{q}}_{\boldsymbol{i}}), \text{with } \underline{b}_i = \begin{bmatrix} b_1^{(i)} & 0 \\ 0 & b_2^{(i)} \end{bmatrix}, \underline{\mu}_i = \begin{bmatrix} \mu_1^{(i)} & 0 \\ 0 & \mu_2^{(i)} \end{bmatrix} \tag{19}$$

In order to guarantee that the kinematic constraints are satisfied during simulation, an asymptotically stable second order dynamics is imposed to $\bar{\boldsymbol{q}}$ and can be solved as described by Baumgarte (1972):

$$\ddot{\bar{\boldsymbol{q}}}(\boldsymbol{q}) + 2\bar{\lambda}\dot{\bar{\boldsymbol{q}}}(\boldsymbol{q}) + \bar{\lambda}^2\bar{\boldsymbol{q}}(\boldsymbol{q}) = \boldsymbol{0} \Longrightarrow \boldsymbol{A}(\boldsymbol{q})\ddot{\boldsymbol{q}} + \boldsymbol{b}(\boldsymbol{q}, \dot{\boldsymbol{q}}) = \boldsymbol{0} \tag{20}$$

$$\text{with } \boldsymbol{b}(\boldsymbol{q}, \dot{\boldsymbol{q}}) = \dot{\boldsymbol{A}}(\boldsymbol{q}, \dot{\boldsymbol{q}})\dot{\boldsymbol{q}} + 2\bar{\lambda}\boldsymbol{A}(\boldsymbol{q})\dot{\boldsymbol{q}} + \bar{\lambda}^2\bar{\boldsymbol{q}}(\boldsymbol{q}) \tag{21}$$

and $\bar{\lambda}$ faster than the robot dynamics.

Now, concatenating the two serial models from Eq. (9) with the end-effector results in:

$$\boldsymbol{f}(\boldsymbol{q}, \dot{\boldsymbol{q}}, \ddot{\boldsymbol{q}}, \boldsymbol{\tau}) = \boldsymbol{\tau} - \boldsymbol{H}(\boldsymbol{q})\ddot{\boldsymbol{q}} - \boldsymbol{h}(\boldsymbol{q}, \dot{\boldsymbol{q}}), \text{ where} \tag{22}$$

$$\boldsymbol{H}(\boldsymbol{q}) = \begin{bmatrix} 0 & 0 & 0 \\ 0 & \boldsymbol{M_1}(\boldsymbol{q_1}) & 0 \\ 0 & 0 & \boldsymbol{M_2}(\boldsymbol{q_2}) \end{bmatrix}, \boldsymbol{h}(\boldsymbol{q}, \dot{\boldsymbol{q}}) = \begin{bmatrix} 0 \\ \boldsymbol{v_1}(\boldsymbol{q_1}, \dot{\boldsymbol{q}}_{\boldsymbol{1}}) + \boldsymbol{g_1}(\boldsymbol{q_1}) + \underline{b}_1\, \dot{\boldsymbol{q}}_{\boldsymbol{1}} + \underline{\mu}_1\, \mathsf{sign}(\dot{\boldsymbol{q}}_{\boldsymbol{1}}) \\ \boldsymbol{v_2}(\boldsymbol{q_2}, \dot{\boldsymbol{q}}_{\boldsymbol{2}}) + \boldsymbol{g_2}(\boldsymbol{q_2}) + \underline{b}_2\, \dot{\boldsymbol{q}}_{\boldsymbol{2}} + \underline{\mu}_2\, \mathsf{sign}(\dot{\boldsymbol{q}}_{\boldsymbol{2}}) \end{bmatrix}, \boldsymbol{\tau} = \begin{bmatrix} 0 \\ \boldsymbol{\tau_1} \\ \boldsymbol{\tau_2} \end{bmatrix}. \tag{23}$$

Applying the VWP to $\boldsymbol{f}(\boldsymbol{q}, \dot{\boldsymbol{q}}, \ddot{\boldsymbol{q}}, \boldsymbol{\tau})$, one gets:

$$\boldsymbol{f}^T(\boldsymbol{q}, \dot{\boldsymbol{q}}, \ddot{\boldsymbol{q}}, \boldsymbol{\tau})\delta\boldsymbol{q} = 0, \tag{24}$$

but it can't be concluded from equation (24) that $\boldsymbol{f}(\boldsymbol{q}) = \boldsymbol{0}$ because the coordinates in the vector $\delta\boldsymbol{q}$ are not independent. To overcome this issue, matrix $\boldsymbol{C}(\boldsymbol{q})$ can be used. Substituting equation (5) in (24) and doing some mathematical manipulation, one gets:

$$\delta\boldsymbol{q_a}^T\boldsymbol{C}^T(\boldsymbol{q})\boldsymbol{f}(\boldsymbol{q}, \dot{\boldsymbol{q}}, \ddot{\boldsymbol{q}}, \boldsymbol{\tau}) = 0 \Longrightarrow \boldsymbol{C}^T(\boldsymbol{q})\boldsymbol{f}(\boldsymbol{q}) = \boldsymbol{0}, \tag{25}$$

which is the forward dynamics equation.

[1] The superscript (i) denotes the i^{th} kinematic chain.

2.4 Inverse Dynamics

Equation (5) shows a relation between the generalized and the actuated coordinates vectors. This same relation can be found for the vectors' derivatives:

$$\dot{\boldsymbol{q}} = \boldsymbol{C}(\boldsymbol{q})\dot{\boldsymbol{q}}_{\boldsymbol{a}}. \tag{26}$$

Differentiating the above equation and substituting it in (25) leads to the inverse dynamics equation:

$$\boldsymbol{H}_{\boldsymbol{a}}(\boldsymbol{q})\ddot{\boldsymbol{q}}_{\boldsymbol{a}} + \boldsymbol{h}_{\boldsymbol{a}}(\boldsymbol{q}, \dot{\boldsymbol{q}}) = \boldsymbol{\tau}_{\boldsymbol{a}}, \tag{27}$$

with

$$\boldsymbol{H}_{\boldsymbol{a}}(\boldsymbol{q}) = \boldsymbol{C}(\boldsymbol{q})^T \boldsymbol{H}(\boldsymbol{q})\boldsymbol{C}(\boldsymbol{q}), \tag{28}$$

$$\boldsymbol{h}_{\boldsymbol{a}}(\boldsymbol{q}, \dot{\boldsymbol{q}}) = \boldsymbol{C}^T(\boldsymbol{q})(\boldsymbol{H}(\boldsymbol{q})\dot{\boldsymbol{C}}(\boldsymbol{q})\dot{\boldsymbol{q}}_{\boldsymbol{a}} + \boldsymbol{h}(\boldsymbol{q}, \dot{\boldsymbol{q}})), \tag{29}$$

$$\boldsymbol{\tau}_{\boldsymbol{a}} = \boldsymbol{C}^T(\boldsymbol{q})\boldsymbol{\tau}. \tag{30}$$

3. CONSTRUCTION

As this robot is idealized for teaching and research purposes, the project focus on reducing the clearances since this is one of the main problems found in the literature that limits the performance of the control methods.

Aiming at this reduction, the motors shouldn't have gearboxes, avoiding backlash and minimizing frictions. As the robot performs only planar movements, all the assembles can be done allowing clearances in directions where the mechanism is not expected to move, or using interference fit if the assemble is in some direction the robot is expected to move.

The main parts of the robot were built using aluminum due to its suitable young module, high resistance, low cost and good machinability. However, it was used a thinner plate of acrylic, this one with lower young modules and resistance to act as a mechanical fuse, avoiding ruptures and enlargement of the holes in the robot's aluminum parts.

As can be seen in Figure 3, the pins were attached to the first link using bolts. The bearings were attached to the second link by interference. The inner rings of the bearings were between nuts and the face of the recessed pin part. The mechanical fuse was also attached by interference generated by tightening the bolts. Thus, once all the attachments were made on the z-axis and everything on x- and y-axis was fixed by interference, the possible clearances are mainly due to plastic deformations of the bearing balls or of the aluminum sheet since they are the most malleable elements.

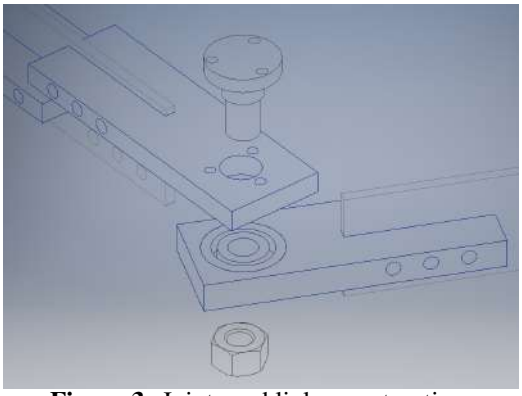

Figure 3: Joints and links construction.

The dimensional synthesis was carried out to avoid the singularity in which both links with length l_2 are aligned while also maximizing the workspace in order to perform tasks with a maximum diameter of 0.10m. Other singularities are mechanically restricted. The construction and the workspace are shown in Figures 1(b) and 2, respectively.

4. RESULTS

In order to test and validate the proposed model, a computed-torque control law, deduced as shown in Slotine and Li (1991) given by:

$$\boldsymbol{\tau}_{\boldsymbol{a}} = \hat{\boldsymbol{H}}_{\boldsymbol{a}}(\boldsymbol{q})(\ddot{\boldsymbol{r}} + 2\lambda\dot{\boldsymbol{e}}_{\boldsymbol{a}} + \lambda^2\boldsymbol{e}_{\boldsymbol{a}}) + \hat{\boldsymbol{h}}_{\boldsymbol{a}}(\boldsymbol{q}, \dot{\boldsymbol{q}}) \tag{31}$$

was implemented, being $\hat{\boldsymbol{H}}_{\boldsymbol{a}}$ and $\hat{\boldsymbol{h}}_{\boldsymbol{a}}$ the estimators of $\boldsymbol{H}_{\boldsymbol{a}}$ and $\boldsymbol{h}_{\boldsymbol{a}}$, respectively. Assuming there are no modeling errors, the resultant closed-loop error dynamics is:

$$\ddot{\boldsymbol{e}}_{\boldsymbol{a}} + 2\lambda\dot{\boldsymbol{e}}_{\boldsymbol{a}} + \lambda^2\boldsymbol{e}_{\boldsymbol{a}} = \boldsymbol{0} \tag{32}$$

where $\boldsymbol{r}$ is the reference signal given in terms of the actuated coordinates and $\boldsymbol{e_a}$ is the actuated coordinates errors defined as $\boldsymbol{e_a} = \boldsymbol{r} - \boldsymbol{q_a}$. λ is a control parameter defined in terms of performance specifications for the linearized system.

Note that for $\hat{\boldsymbol{h}}_{\boldsymbol{a}} = \boldsymbol{0}$ and $\hat{\boldsymbol{H}}_{\boldsymbol{a}} = m^* \boldsymbol{I}$, the control law is equivalent to a PD with feed-forward acceleration.

4.1 Simulation Results

The estimated values for the parameters of the serial subsystems that compose the parallel mechanism are presented in Tables 1 and 2. The end-effector mass is considered null. Measurements of the link lengths and the distance between the actuators validated the proposed design values. The parameters concerning inertial data such as mass and its center of gravity and moment of inertia were obtained through the mechanism CAD model.

Table 1: Parameters of the first serial chain.

Parameters	Values	Units
l_0	0.050	m
l_1	0.120	m
l_2	0.160	m
l_{g1}	0.060	m
l_{g2}	0.078	m
m_1	0.062	kg
m_2	0.124	kg
J_{z1}	$1.073 \cdot 10^{-4}$	$kg.m^2$
J_{z2}	$4.380 \cdot 10^{-4}$	$kg.m^2$
b_1	$1.226 \cdot 10^{-4}$	$N.m.s/rad$
μ_1	$4.357 \cdot 10^{-2}$	$N.m$

Table 2: Parameters of the second serial chain.

Parameters	Values	Units
l_0	0.050	m
l_1	0.120	m
l_2	0.160	m
l_{g1}	0.060	m
l_{g2}	0.058	m
m_1	0.062	kg
m_2	0.097	kg
J_{z1}	$2.960 \cdot 10^{-4}$	$kg.m^2$
J_{z2}	$9.800 \cdot 10^{-4}$	$kg.m^2$
b_1	$2.039 \cdot 10^{-4}$	$N.m.s/rad$
μ_1	$4.992 \cdot 10^{-2}$	$N.m$

As the friction coefficients were not measured in the passive joints, b_2 and μ_2 are considered null for both serial chains.

The reference trajectory is a circular path with 1 second period simulated for a total of 8 cycles followed by a sudden stop. Its expression is given by (33). The mechanism always starts from the rest, and its initial position is $(x, y) = (-0.002, 0.108)\, m$.

$$\begin{cases} x_d(t) = -0.05\cos(2\pi t) \\ y_d(t) = 0.158 - 0.05\sin(2\pi t) \end{cases} \tag{33}$$

Using the CTC law (31) with $\lambda = 60$ rad/s and supposing no error on the estimated parameters but the estimated Coulomb frictions – which are set to zero – the following results are obtained through direct dynamic simulation (Figure 4):

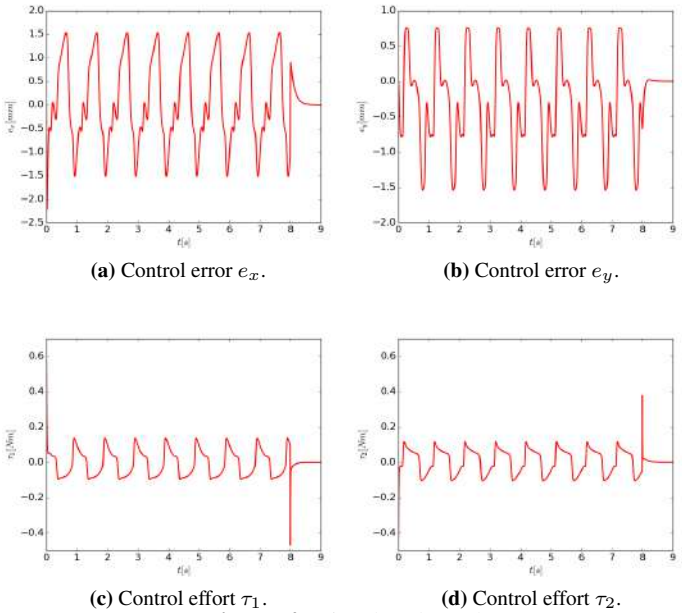

(a) Control error e_x. **(b)** Control error e_y.

(c) Control effort τ_1. **(d)** Control effort τ_2.

Figure 4: Simulated results.

4.2 Experimental Results

The parameters of the position controllers used in the experimental tests are shown in Table 3.

Table 3: Parameters of the position controllers in the joint space.

Strategy	$\lambda[rad/s]$	$m^*[kg.m^2]$
PD	35	$3.58 \cdot 10^{-3}$
CTC	60	-

Figures 5 and 6 present the trajectory follow-up graphs and the time history of both control errors and efforts for the PD controller with feed-forward acceleration and the computed-torque control, respectively. Performance comparisons are presented in Table 4.

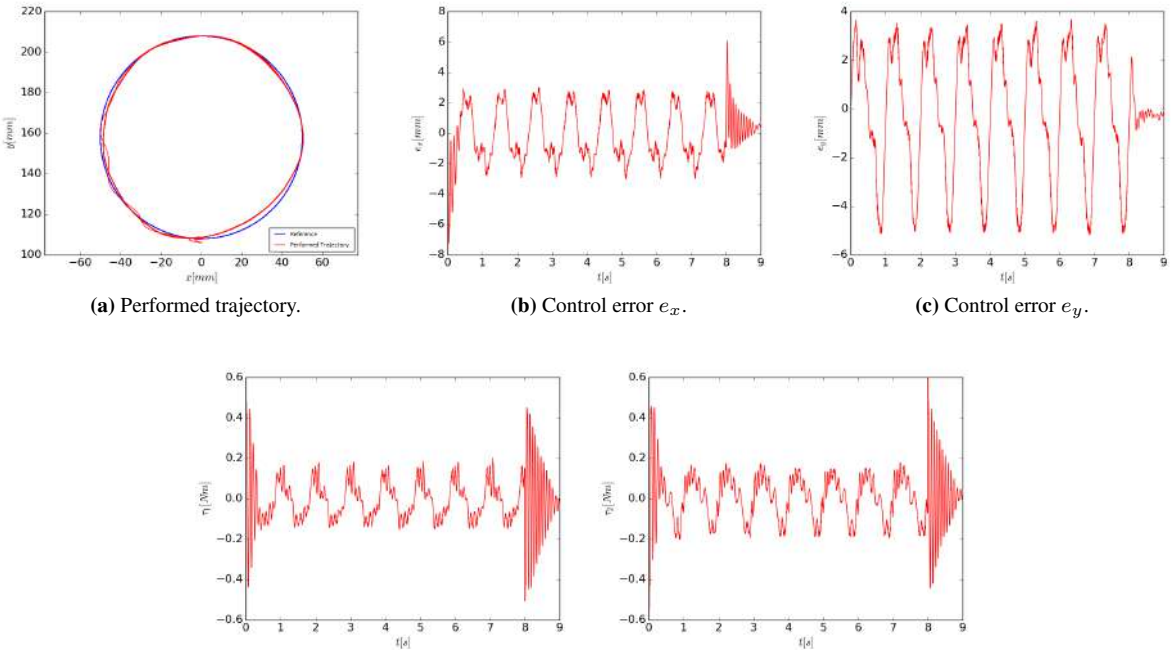

(a) Performed trajectory. **(b)** Control error e_x. **(c)** Control error e_y.

(d) Control effort τ_1. **(e)** Control effort τ_2.

Figure 5: Experimental results – PD controller.

Figure 5 shows that the resultant output (in red) tracks the reference trajectory (in blue) with a maximum error of approximately 3 mm in x and up to 5 mm in y, presenting larger values at the beginning and at the end of the trajectory due to the sudden entry of the control signal, leading to more than 6 mm of error in x. The control efforts remain between ± 0.2 N.m in both axes, except for the beginning and the end of the trajectory where they reach peaks of more than ± 0.4 N.m in both axes.

Figure 6 shows that the CTC present a trajectory tracking with a maximum error of approximately 2 mm in x and up to 1.3 mm in y, also presenting larger values at the beginning and at the end of the trajectory due to the same reasons as the PD controller, leading to more than 8 mm of error in x and 3.5 mm in y. The control efforts remain between ± 0.4 N.m in both axes, except for the beginning and the end of the trajectory where they reach peaks of more than ± 0.5 N.m in x and ± 0.6 N.m in y.

Table 4 presents the RMS values of position errors and control efforts in the circular trajectory for each control strategy, which are calculated as follows:

$$e_{RMS} = \sqrt{\frac{1}{N}\sum_{k=1}^{N} e_x^2[k] + e_y^2[k]} \tag{34}$$

$$\tau_{RMS} = \sqrt{\frac{1}{N}\sum_{k=1}^{N} \tau_1^2[k] + \tau_2^2[k]} \tag{35}$$

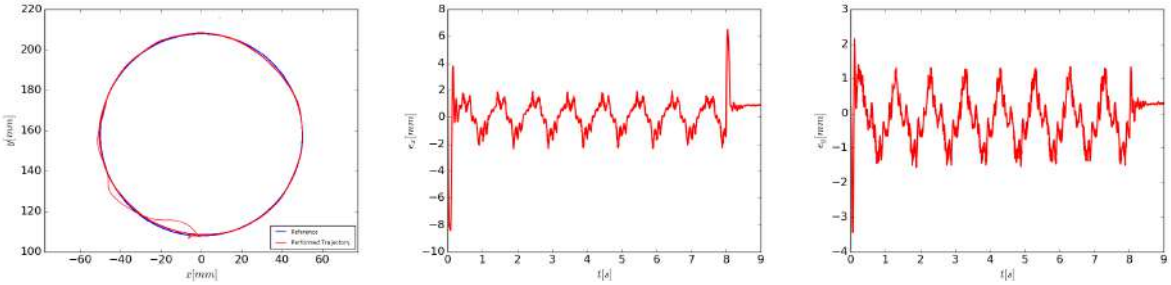

(a) Performed trajectory. **(b)** Control error e_x. **(c)** Control error e_y.

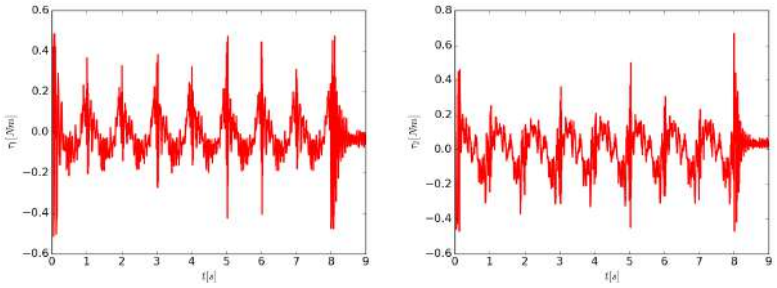

(d) Control effort τ_1. **(e)** Control effort τ_2.

Figure 6: Experimental results – CTC controller.

Table 4: RMS error and control effort values (steady state) and Position stationary error

Strategy	$e_{RMS}[mm]$	$\tau_{RMS}[kg.m^2]$	$e_x[mm]$	$e_y[mm]$	$e[mm]$
PD	3.15	0.132	0.444	-0.195	0.484
CTC	1.14	0.143	0.903	0.289	0.949

and also presents the positional error values, which means the position error value after the manipulator completes the trajectory and stabilizes at a fixed point. The error value e of the fifth column is obtained by making $e = \sqrt{e_x^2 + e_y^2}$. In other words, the distance between the desired and actual positions of the end-effector.

Gathering the information presented in all trajectory follow-up and time history graphs with the ones accounted in the comparative tables exhibited earlier, some conclusions can be drawn about the implemented control techniques.

Analyzing Table 4, it can be observed that the CTC presents an RMS error 76% lower than the PD at a cost of an energy expenditure only 8% higher. This substantiates that, as expected, the model-based control is far superior than the non model-based control in performance, which also indicates that the deduced model is representative.

Comparing now Figures 5(a-c) with Figures 6(a-c), a much smoother behavior can be perceived in the trajectory path using the PD controller. In addition, Table 4 shows that the position stationary error (after the trajectory was finished) is higher with the CTC. This happens due to the proximity of the trajectory starting point, which is the same at the end, to a region of kinematic singularities. In these regions, the components of the matrix $\hat{\boldsymbol{H}}_{\boldsymbol{a}}$ for the CTC reach high values, which means there is a high control gain that slightly compromises the stability of the system while that same matrix remains constant for the PD controller.

5. CONCLUSION

In this paper, a generic methodology for modeling parallel mechanisms based on the concept of subsystem coupling is proposed. From a previously deduced model of its serial chains and the kinematic links between them and the end-effector, the dynamic model of a 5R type parallel mechanism is obtained. Considering the deduced model, direct dynamic simulation and an experimental position control tests are performed with a model-based control technique. The results obtained validate the fidelity of the deduced model for position tracking through model-based control design, which proved to be superior than the non model-based controller in the subject of control error effective value at a cost of a small increase in the energy consumption.

It can be concluded that the computed-torque control technique is quite adequate and effective in performing position control of parallel mechanisms when using reliable models of the system. In addition, the modeling method used proved to be effective since it can reuse previously designed models, which simplifies and streamlines the modeling task.

6. ACKNOWLEDGEMENTS

This study was supported by the Coordenação de Aperfeiçoamento de Pessoal de Nível Superior - Brasil (CAPES) – Finance Codes 00188882.333338/2019-01 and 88882.377489/2019-01 and by the Conselho Nacional de Desenvolvimento Científico e Tecnológico (CNPq) – Finance Code 162502/2015-0.

7. REFERENCES

Abdellatif, H. and Heimann, B., 2009. "Computational efficient inverse dynamics of 6-dof fully parallel manipulators by using the lagrangian formalism". *Mechanism and Machine Theory*, Vol. 44, No. 1, pp. 192–207.

Akbarzadeh, A., Enferadi, J. and Sharifnia, M., 2013. "Dynamics analysis of a 3-rrp spherical parallel manipulator using the natural orthogonal complement". *Multibody System Dynamics*, Vol. 29, No. 4, pp. 361–380.

Almeida, R., 2013. *Modelagem dinâmica e controle de robô manipulador de arquitetura paralela assimétrica de três graus de liberdade. 2013. 179 p.* Ph.D. thesis, Tese (Doutorado em Engenharia Mecânica)-Escola Politécnica, Universidade de São Paulo.

Altuzarra, O., Eggers, P.M., Campa, F.J., Roldan-Paraponiaris, C. and Pinto, C., 2015. "Dynamic modelling of lower-mobility parallel manipulators using the boltzmann-hamel equations". In *Mechanisms, Transmissions and Applications*, Springer, pp. 157–165.

Arian, A., Danaei, B., Abdi, H. and Nahavandi, S., 2017. "Kinematic and dynamic analysis of the gantry-tau, a 3-dof translational parallel manipulator". *Applied Mathematical Modelling*, Vol. 51, pp. 217–231.

Baumgarte, J., 1972. "Stabilization of constraints and integrals of motion in dynamical systems." *Computer Methods in Applied Mechanics and Engineering*, Vol. 1, pp. 1–16.

Carp-Ciocardia, D. *et al.*, 2003. "Dynamic analysis of clavel's delta parallel robot". In *2003 IEEE International Conference on Robotics and Automation (Cat. No. 03CH37422)*. IEEE, Vol. 3, pp. 4116–4121.

Cheng, H., Yiu, Y.K. and Li, Z., 2003. "Dynamics and control of redundantly actuated parallel manipulators". *IEEE/ASME Transactions on mechatronics*, Vol. 8, No. 4, pp. 483–491.

Codourey, A., 1996. "Dynamic modelling and mass matrix evaluation of the delta parallel robot for axes decoupling control". In *Proceedings of IEEE/RSJ International Conference on Intelligent Robots and Systems. IROS'96*. IEEE, Vol. 3, pp. 1211–1218.

Codourey, A. and Burdet, E., 1997. "A body-oriented method for finding a linear form of the dynamic equation of fully parallel robots". In *Proceedings of International Conference on Robotics and Automation*. IEEE, Vol. 2, pp. 1612–1618.

Craig, J.J., 2005. *Introduction to robotics: mechanics and control*. Addison-Wesley series in electrical and computer engineering: control engineering, 3rd edition.

Dasgupta, B. and Mruthyunjaya, T., 1998. "A newton-euler formulation for the inverse dynamics of the stewart platform manipulator". *Mechanism and machine theory*, Vol. 33, No. 8, pp. 1135–1152.

Gallardo-Alvarado, J., Rodríguez-Castro, R. and Delossantos-Lara, P.J., 2018. "Kinematics and dynamics of a 4-prur schönflies parallel manipulator by means of screw theory and the principle of virtual work". *Mechanism and Machine Theory*, Vol. 122, pp. 347–360.

Geike, T. and McPhee, J., 2003. "Inverse dynamic analysis of parallel manipulators with full mobility". *Mechanism and Machine Theory*, Vol. 38, No. 6, pp. 549–562.

Khalil, W. and Dombre, E., 2004. *Modeling, identification and control of robots*. Butterworth-Heinemann.

Khan, W.A., Krovi, V.N., Saha, S.K. and Angeles, J., 2005. "Recursive kinematics and inverse dynamics for a planar 3r parallel manipulator". *Journal of Dynamic Systems, Measurement, and Control*, Vol. 127, No. 4, pp. 529–536.

Lanczos, C., 2012. *The variational principles of mechanics*. Courier Corporation. ISBN 0-486-65067-7.

Li, Y. and Staicu, S., 2012. "Inverse dynamics of a 3-prc parallel kinematic machine". *Nonlinear Dynamics*, Vol. 67, No. 2, pp. 1031–1041.

Li, Y. and Xu, Q., 2005. "Kinematics and inverse dynamics analysis for a general 3-prs spatial parallel mechanism". *Robotica*, Vol. 23, No. 2, pp. 219–229.

Li, Y. and Xu, Q., 2009. "Dynamic modeling and robust control of a 3-prc translational parallel kinematic machine". *Robotics and Computer-Integrated Manufacturing*, Vol. 25, No. 3, pp. 630–640.

Li, Y.W., Wang, J.S., Wang, L.P. and Liu, X.J., 2003. "Inverse dynamics and simulation of a 3-dof spatial parallel manipulator". In *2003 IEEE International Conference on Robotics and Automation (Cat. No. 03CH37422)*. IEEE, Vol. 3, pp. 4092–4097.

Merlet, J.P., 2002. "Still a long way to go on the road for parallel mechanisms". In *Proc. ASME 2002 DETC Conf., Montreal*.

Orsino, R.M.M., 2016. *A contribution on modeling methodologies for multibody systems*. Ph.D. thesis, PhD thesis, São Paulo, Brazil: University of São Paulo. See http://www. teses. usp. br/teses/disponiveis/3/3151/tde-22062016-160724/en. php.

Orsino, R.M.M., Coutinho, A.G. and Coelho, T.A.H., 2016. *Dynamic Modelling and Control of Balanced Parallel Mechanisms*, Springer International Publishing, Cham, pp. 403–445. ISBN 978-3-319-17683-3.

Orsino, R.M.M. and Hess-Coelho, T.A., 2015. "A contribution on the modular modelling of multibody systems". *Proc. R. Soc. A*, Vol. 471, No. 2183, p. 20150080.

Orsino, R.M.M., Hess-Coelho, T.A. and Pesce, C.P., 2015. "Analytical mechanics approaches in the dynamic modelling of delta mechanism". *Robotica*, Vol. 33, No. 4, pp. 953–973.

Pashkevich, A., Chablat, D. and Wenger, P., 2006. "Kinematics and workspace analysis of a three-axis parallel manipulator: the orthoglide". *Robotica*, Vol. 24, No. 1, pp. 39–49.

Shiau, T.N., Tsai, Y.J. and Tsai, M.S., 2008. "Nonlinear dynamic analysis of a parallel mechanism with consideration of joint effects". *Mechanism and Machine Theory*, Vol. 43, No. 4, pp. 491–505.

Singh, Y. and Santhakumar, M., 2015. "Inverse dynamics and robust sliding mode control of a planar parallel (2-prp and 1-ppr) robot augmented with a nonlinear disturbance observer". *Mechanism and Machine Theory*, Vol. 92, pp. 29–50.

Singh, Y., Vinoth, V., Kiran, Y.R., Mohanta, J.K. and Mohan, S., 2015. "Inverse dynamics and control of a 3-dof planar parallel (u-shaped 3-ppr) manipulator". *Robotics and Computer-Integrated Manufacturing*, Vol. 34, pp. 164–179.

Singh, Y., Vinoth, V. and Santhakumar, M., 2014. "Dynamic modellingand control of a 3-dof planar parallel robotic (xyθz motion) platform". *Procedia Materials Science*, Vol. 5, pp. 1528–1539.

Slotine, J.J.E. and Li, W., 1991. *Applied nonlinear control*. 3rd edition.

Staicu, S., 2009a. "Inverse dynamics of the 3-prr planar parallel robot". *Robotics and Autonomous Systems*, Vol. 57, No. 5, pp. 556–563.

Staicu, S., 2009b. "Recursive modelling in dynamics of agile wrist spherical parallel robot". *Robotics and Computer-Integrated Manufacturing*, Vol. 25, No. 2, pp. 409–416.

Staicu, S., 2009c. "Recursive modelling in dynamics of delta parallel robot". *Robotica*, Vol. 27, No. 2, pp. 199–207.

Staicu, S., Liu, X.J. and Wang, J., 2007. "Inverse dynamics of the half parallel manipulator with revolute actuators". *Nonlinear Dynamics*, Vol. 50, No. 1-2, pp. 1–12.

Staicu, S. and Zhang, D., 2008. "A novel dynamic modelling approach for parallel mechanisms analysis". *Robotics and Computer-Integrated Manufacturing*, Vol. 24, No. 1, pp. 167–172.

Staicu, S., Zhang, D. and Rugescu, R., 2006. "Dynamic modelling of a 3-dof parallel manipulator using recursive matrix relations". *Robotica*, Vol. 24, No. 1, pp. 125–130.

Tarcisio A.H. Coelho, Liang Yong, V.F.A., 2004. "Decoupling of dynamic equations by means of adaptive balancing of 2-dof open-loop mechanisms". *Mechanism and Machine Theory*, Vol. 39, pp. 871–881.

Tsai, L.W., 1999. *Robot analysis: the mechanics of serial and parallel manipulators*. John Wiley & Sons.

Wu, J., Wang, J., Wang, L. and Li, T., 2009. "Dynamics and control of a planar 3-dof parallel manipulator with actuation redundancy". *Mechanism and Machine Theory*, Vol. 44, No. 4, pp. 835–849.

Xi, F. and Sinatra, R., 2002. "Inverse dynamics of hexapods using the natural orthogonal complement method". *Journal of manufacturing systems*, Vol. 21, No. 2, pp. 73–82.

Yao, J., Gu, W., Feng, Z., Chen, L., Xu, Y. and Zhao, Y., 2017. "Dynamic analysis and driving force optimization of a 5-dof parallel manipulator with redundant actuation". *Robotics and Computer-Integrated Manufacturing*, Vol. 48, pp. 51–58.

Zhang, X., Zhang, X. and Chen, Z., 2014. "Dynamic analysis of a 3-rrr parallel mechanism with multiple clearance joints". *Mechanism and Machine Theory*, Vol. 78, pp. 105–115.

Zhao, Y. and Gao, F., 2009a. "Dynamic formulation and performance evaluation of the redundant parallel manipulator". *Robotics and Computer-Integrated Manufacturing*, Vol. 25, No. 4-5, pp. 770–781.

Zhao, Y. and Gao, F., 2009b. "Inverse dynamics of the 6-dof out-parallel manipulator by means of the principle of virtual work". *Robotica*, Vol. 27, No. 2, pp. 259–268.

Zhu, Z., Li, J., Gan, Z. and Zhang, H., 2005. "Kinematic and dynamic modelling for real-time control of tau parallel robot". *Mechanism and machine theory*, Vol. 40, No. 9, pp. 1051–1067.